# Confocal XANES and the Attic Black Glaze: The Three-Stage Firing Process through Modern Reproduction

**ARTICLE** *in* ANALYTICAL CHEMISTRY · JUNE 2014

Impact Factor: 5.64 · DOI: 10.1021/ac500990k · Source: PubMed

analytical chemistry

Article

pubs.acs.org/ac

# Confocal XANES and the Attic Black Glaze: The Three-Stage Firing Process through Modern Reproduction

Lars Lühl,*[,†,¶,⊥] Bernhard Hesse,[†,∥] Ioanna Mantouvalou,[†] Max Wilke,[‡] Sammia Mahlkow,[†] Eleni Aloupi-Siotis,[§,⊥] and Birgit Kanngiesser[†]

[†]Technische Universität Berlin, Hardenbergstrasse 36, 10623 Berlin, Germany

[‡]Deutsches Geoforschungszentrum, Telegrafenberg, 14473 Potsdam, Germany

[§]Thetis Authentics Ltd., 4 Diagoras, GR-116 36 Athens, Greece

Supporting Information

**ABSTRACT:** The decorated black- and red-figured Athenian vases (sixth and fifth century BC) and the plain black-glazed ware represent a milestone in our material culture due to their aesthetic and technological value; the Attic black glaze is of particular interest since it is a highly resistant potash–alumino–silicate glass, colored by magnetite nanocrystals (<200 nm). This study presents a new methodological approach for correlating the iron oxidation state in the black glaze layer with the manufacturing process by means of conventional and confocal X-ray absorption near edge spectroscopy (XANES). The enhanced surface sensitivity of confocal XANES is combined with conventional XANES resulting in higher counting rates to reliably evaluate the iron oxidation state ($Fe^{3+}/\Sigma Fe$) of the surface layer. A detailed description of the new evaluation procedure is presented. The three-stage firing process was retraced by correlating selected attic black-glazed (BG) specimens from different periods (Archaic, Classical, Hellenistic) with laboratory reproductions. The modern BG specimens serving as reference samples were produced by following the three-stage firing process (i.e., under oxidizing–reducing–oxidizing (ORO) conditions) at different top temperatures, using clay suspensions of different particle size produced with treatment of raw illitic clays from Attica.

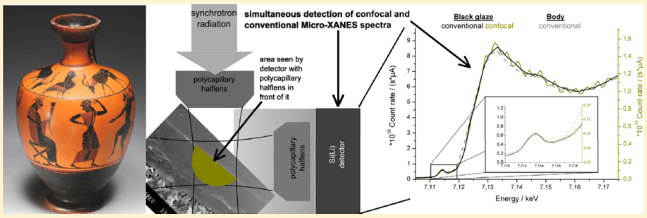


X-ray absorption near edge spectroscopy (XANES) has proven to be a useful tool for the nondestructive investigation of the oxidation state of elements during the last decades. In particular the shape of the pre-edge structure[1] in K-edge XANES spectra shows a high sensitivity to oxidation state and coordination. Wilke et al. developed in their work a methodology for determining the iron oxidation state in minerals and glass focusing on the pre-edge of Fe K-edge XANES spectra that was obtained by analysis of an extensive set of reference samples.[2,3] In the work of Berry et al.[4] on XANES calibrations for the oxidation state of iron in silicate glasses, advantages of the technique over Mössbauer spectroscopy (analysis of bulk materials only), EELS using TEM (nanoscale analysis, limitations due to melt inclusions, invasive sample preparation), and XPS (complicated by surface sensitivity and the need for ultrahigh vacuum techniques) were discussed. The present study relies on the methodology developed by Wilke et al.,[2,3] while taking into account previous qualitative data on the application of Fe L- and K-edge XAS on black-glazed ware from Northern Etruria[5] and the nondestructive synchrotron radiation-XAS on decorated Attic pottery from the south of Italy and Sicily[6] that compares well with previous data obtained by Mössbauer spectroscopy.[7,8]

Attic black- and red-figure vases and plain black-glazed ware form a milestone in the evolution of material culture due to their special manufacturing process and technological features (see Figure 1a) beyond their aesthetic appeal and historical value. Attic pottery consists of a porous ceramic body with a reddish-brown color and a glassy black layer on top (see Figure 1b), both containing iron.[9−16] The black glaze is produced with the use of a special clay paint[17,18] which is applied on the surface of the clay vase. Following a three-stage firing process under oxidizing–reducing–reoxidizing (ORO) conditions, it turns to a vitrified black layer (see Figure 1c) well adhered to the reddish-brown ceramic body. This technique known as the "iron reduction technique' reached perfection during the classical times in Attica though it was also practiced in other production centers in the mainland Greece (Boeotia, Euboea, Laconia, and Thessaly) and the Greek colonies (especially in southern Italy).

The aim of the present study was to correlate the oxidation state of iron in the black glaze of the pottery to the degree of refinement of the used clay suspension and firing conditions by investigating modern reproductions prepared under controlled conditions at the THETIS' production workshop (Athens).[18] The results are correlated with those received from the analysis of selected ancient specimens from recent excavations in the

**Received:** February 23, 2014
**Accepted:** June 3, 2014
**Published:** June 6, 2014

   dx.doi.org/10.1021/ac500990k | *Anal. Chem.* 2014, 86, 6924−6930

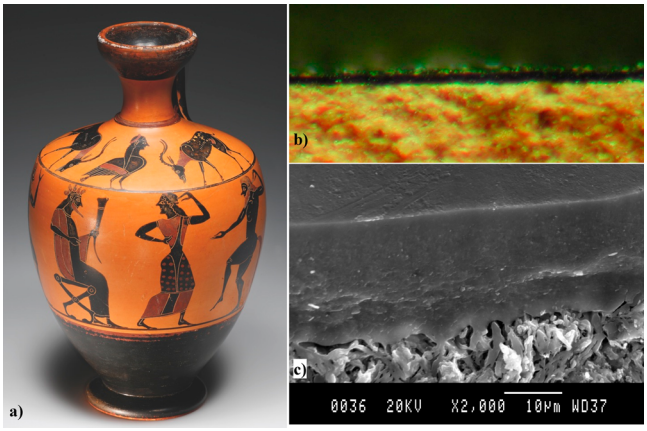


**Figure 1.** (a) Black-figure shoulder lekythos, attributed to the Taleides Painter, Attic, ca. 550−540 BC, Cahn Auktionen AG Basel (A.6/5 Nov.2011 Lot 74), (b) optical microscope image of a cross section of a modern BG reproduction showing the glassy black layer over the reddish-brown porous bulk, (c) SEM image of a BG attic sherd, cross section fresh fracture surface 2000×; dense micromorphology, glassy on top and near the body, flaky in the middle zone.

center of Athens (New Acropolis Museum and Kerameikos area). This research work is the first step to further investigate the development of the attic pottery production over time, from subgeometric (9th century BC) to late Hellenistic period (2nd century BC) by analyzing a large number of well-documented sherds from Attica.

For the XANES measurements a novel measurement strategy adapted to the peculiarities of the specimens had to be developed. The impact of the ceramic body on the determination of the iron oxidation state of the black glaze had to be excluded, and absorption effects to be taken into account.

**The Attic Black Glaze and the Three-Stage Firing.** In modern physicochemical terms the Attic black glaze (BG) can be described as a potassium−aluminosilicate glass colored by magnetite nanocrystals (particle size <200 nm) synthesized in situ during the three-stage ORO firing of a colloidal suspension of a ferruginous illitic clay with low CaO content (<1%). The average composition of the glaze in wt % as determined by 26 samples is $SiO_2$ 46, 2 (±1, 3); $Al_2O_3$ 30, 0 (±1, 1); FeO 14, 5 (±1, 6); $K_2O$ 5, 4 (±1, 1) ; $Na_2O$ 0, 7 (±0, 2); MgO 1, 9 (±0, 3); CaO 0, 8 (±0, 3); $TiO_2$ 0, 6 (±0, 3).[16−18] The iron oxidation state is an indicator for the three-stage firing process detailed as follows: during the first stage, involving a temperature increase to a $T_{max}$ of 870−950 °C under oxidation conditions, the iron oxides and/or hydroxides contained in both the clay body and the paint layer turn into Fe(III) oxide, hematite $Fe_2O_3$. At $T_{max}$ the kiln slits are closed, and green wood, which burns incompletely providing a reducing atmosphere, is placed inside. Under reducing conditions partial reduction of hematite occurs forming $Fe^{2+}$ compounds, i.e., magnetite ($FeO{\cdot}Fe_2O_3$), hercynite ($FeO{\cdot}Al_2O_3$), and wustite (FeO), and thus the glossy black glaze is formed. At this stage the temperature decreases[17,18] due to incomplete combustion of the burning material. In the third stage, by opening the slits of the kiln again the oxygen penetrates the porous ceramic body, and hematite is formed again while the glaze layer remains black since it is impermeable to oxygen. The exact nature of the Attic BG has become the subject of several studies especially in view of its degree of vitrification; as shown in Figure 1c, the BG layer under the SEM is not totally vitrified. Alhough it exhibits a glassy micromorphology near the external surface and in the interface with the clay body, in the middle zone it retains a flaky appearance due to incomplete melting of the clay platelets. This is clearly visible in the SEM image of Figure 2, showing a BG modern reproduction at 120 000×,

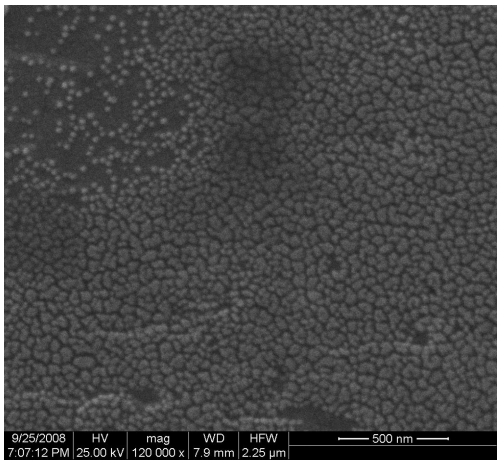


**Figure 2.** SEM image of a modern BG sherd, cross section fresh fracture surface, magnification 120 000×; "clay" nanoparticles with rounded edges are still visible before diffusing in the glassy phase.

where numerous sintered "clay" nanoparticles during glaze formation are clearly visible. Over the past 80 years a series of studies have been conducted dealing with the understanding, analytical characterization, and modern reproduction of the Attic BG.[8−17] However, there are still technological details to be defined; more specifically the influence of the maximum firing temperature and of the particle size of the clay suspension used for the production of the BG on the exact oxidation state of the iron and, thus, also on the appearance (i.e., coloration) of the black glaze is not fully understood, yet.

**The New XANES Methodological Approach.** Strong effort was made to develop a nondestructive analytical tool to be able to apply XANES on more valuable decorated sherds in the future. Hence, the XANES spectra had to be acquired in fluorescence mode.[19] Figure 3a illustrates a typical setup for

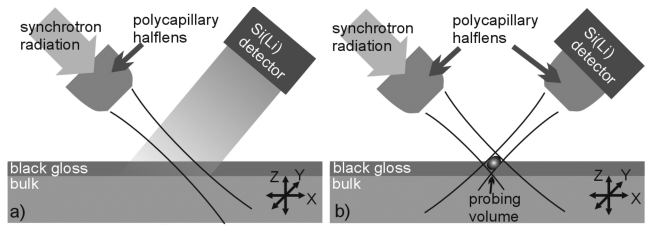


**Figure 3.** (a) Sketch of conventional and (b) confocal setup for XANES in fluorescence mode.

"conventional" XANES in fluorescence mode in 45°/45° geometry. The spectra collected represent depth-integrated information. To evaluate the contribution of the ceramic body on the spectra, we additionally performed measurements in confocal geometry. The confocal setup was initially developed for depth-resolved elemental mapping. However, it also allows the collection of depth-resolved XANES spectra (Figure 3b). A detailed description of the confocal setup is given by Malzer et


dx.doi.org/10.1021/ac500990k | Anal. Chem. 2014, 86, 6924−6930

al.[20] and Mantouvalou et al.[21] Recently, we developed a depth-resolved confocal XANES analysis including correction of absorption effects for layered structures.[22]

Also for XANES spectra acquired in conventional mode without a second lens in front of the detector, appropriate absorption corrections have to be performed. For homogeneous samples, analyzed by conventional XANES in fluorescence mode, several procedures exist to correct absorption effects in the detected spectra.[23−26] Nevertheless, these procedures are not applicable to attic pottery without constrains due to the layered structure of the samples as shown in the optical microscopy and SEM micrographs of Figures 1b and 1c referring to a modern reproduction and an ancient sherd, respectively.

Therefore, we provide a combined methodological approach for micro-XANES analysis of an analyte with stratified structures considering absorption effects for both conventional and confocal setups. Appropriate measures that have to be taken for the various steps of the experimental part as well as for the data evaluation part are considered and explained.

## INSTRUMENTATION

The experiments were carried out at the $\mu$Spot beamline of Berlin's synchrotron radiation facility BESSY II.[27,28] The incoming X-ray beam is focused with a polycapillary half-lens producing a spot size of about 30 $\mu$m fwhm$_E$ on the sample at the iron K-edge energy. The fluorescence intensity is detected with a seven-element Si(Li) detector. The seven detector elements are aligned on a surface of a sphere pointing to the same position on the sample with equal distances to the focus.

In front of the topmost detector element, a second polycapillary half-lens is placed with fwhm$_D$ of 18 $\mu$m at the iron K$\alpha$ fluorescence line energy. After alignment in terms of maximum overlap of both foci, the width of the formed probing volume normal to the sample surface was determined following the calibration procedure for confocal micro-XANES[8] to be $\sigma_x$ = (14.1 ± 0.2) $\mu$m, corresponding to a fwhm$_x$ of (33.2 ± 0.5) $\mu$m.

A sufficient spectral resolution for XANES measurements is provided by a Si(311) double-crystal monochromator with an approximate energy resolution of $E/\Delta E \approx 25\,000$.

**Samples Description.** Modern reproductions were produced following the manufacturing process developed by Aloupi (1993)[17,18] using different clays for the bulk and black glaze and a three-step firing process, involving a decrease of temperature during reduction, as described in The Attic Black Glaze and the Three-Stage Firing. Modern reproductions were produced at three maximum temperatures (0: raw material, 1: 870 °C, 2: 890 °C, and 3: 930 °C) using three different fractions of an illitic ferruginous clay suspended in water in order to study their dependence on the amount of $Fe^{3+}$ and on the appearance of the black glaze (Table 3). The gradually increasing particle size of the three fractions received from the clay−water system is expressed for convenience with the equivalent spherical diameter (ESD) A: <0.3 $\mu$m, B: <0.8 $\mu$m, and C: <5.5 $\mu$m). Particle size analysis (dynamic light scattering_DLS) of the three clay fractions has shown frequency distributions around 220−330, 560−770, and 5300−5500 nm; the frequency distributions by intensity expressing the total surface area for the three clay suspensions are compatible with their ESD, i.e., A (<0.3 $\mu$m): 331 nm 100%, B (<0.8 $\mu$m): 703 nm 97%, 5340 nm 3%, C (<5.5 $\mu$m): 653 nm 68%, 5494 nm 32% .

Three Attic sherds from recent excavations in the center of Athens were selected for the analysis; ARCH-ACROP-2 and HEL-ACROP-5 originate from the area of Makriyanni (new Acropolis Museum) while CL-KER-20 originates from the area near ancient Kerameikos. All three sherds have a thick and uniform BG layer without visible defects under the stereoscope. The cross sections of all specimens, i.e., ancient sherds and modern reproductions, were examined by SEM in order to measure the thicknesses of the glaze layer, revealing layer thicknesses between 21 and 32 $\mu$m (Figure 1c), which is in line with previous studies by others reporting black glaze thicknesses between 10 and 40 $\mu$m.[29] The BG sherds analyzed here were chosen among a set of 12 Attic BG samples which had been analyzed under slightly different experimental conditions in the beginning of the project; this data set formed the basis for the present analytical setup though a detailed account and has been omitted for convenience.

**XANES Measurements.** The scanned energy region for XANES measurements presented ranges from 7006 to 7406 eV. This energy range is split into four subranges with different step sizes and different acquisition times (Table 1). Settings were set such that the number of counts in the maximum of the pre-edge for the conventional detector element was higher than 30 000. The extended region was only used for normalization purposes.

**Table 1. Energy Regions with Step Widths and Acquisition Times**

| part | energy region, eV | step width, eV | measurement time, s |
|---|---|---|---|
| 1 (offset) | 7006.28−7106.28 | 10 | 10−20 |
| 2 (pre-edge) | 7106.28−7118.28 | 0.15 | 40−130 |
| 3 (XANES) | 7118.28−7172.28 | 0.5 | 15−40 |
| 3 (extended region) | 7172.28−7406.28 | 10 | 10−20 |

**Measurement Strategy.** XANES spectra were detected by all seven detector elements simultaneously. For each spatial position of the probing volume, the confocal signal of the topmost detector element was collected at the same time as the bulk signals of the other six detector elements. The bottom detector element is aligned in the same geometry with respect to sample surface compared to the topmost element (see also the Supporting Information). Results shown here for conventional XANES refer to the measured spectra detected with the bottom detector to exclude different geometry effects in the conventional and confocal spectra.

First, depth profiles were obtained by moving the sample stepwise into the probing volume for excitation energies above the Fe absorption edge (here 7119 or 7200 eV) and monitoring the iron fluorescence intensity detected with the confocal detector element.[30] Afterward, surface micro-XANES measurements of the black glaze top layer were carried out. To achieve this with signals collected only from the black glaze layer, the sample was moved to the motor position corresponding to the half of the maximum intensity of the depth scan in order to place only about half of the probing volume inside the black glaze. Using the quantification procedure for confocal micro-XRF developed by Mantouvalou et al.[21] for reconstructing stratified structures, successive calculations revealed that the position of the center of the probing volume was approximately 5 $\mu$m in front of the sample surface.


dx.doi.org/10.1021/ac500990k | Anal. Chem. 2014, 86, 6924−6930

Defining the extension of the whole probing volume in scanning direction to be at least 95% of the Gaussian distribution $(4*\sigma_x)$[22] results in a probing volume of 56 $\mu$m. Thus, for measurement positions at half of the maximum intensity of the depth profile, the probing volume intrudes approximately 23 $\mu$m ((56 $\mu$m)/2−5 $\mu$m) into the samples.

Because the black glaze thickness of our samples is at minimum 21 $\mu$m, surface measurements guarantee that only signal originating from the black glaze is detected in confocal micro-XANES spectra excluding interference of the ceramic body. Considerations about measurements of the black glaze with thicknesses in the range of 10 $\mu$m are discussed later.

In comparison to confocal micro-XANES, conventional micro-XANES yields integrated information from the surface as well as from the depth but with considerably higher counting rates. This is due to the restricted transmission of the second lens in the confocal mode, which reduces the confocal signal.[31] Furthermore, the size of the probing volume and its overlap with the sample is limited resulting in reduced detected fluorescence intensity.

In case of identical spectra, the higher count rates of conventional XANES spectra can be used for further calculations but different absorption effects have to be taken into account, which will be elaborated in the following section.

## QUANTIFICATION

Quantitative determination of the $Fe^{3+}/Fe$ ratio, whether from conventional or confocal micro-XANES, is based on the detailed analysis of the pre-edge region. The spectral evaluation is very sensitive to the normalization and background subtraction which is therefore described in the Supporting Information in detail.

After background subtraction the pre-edges are fitted with two Gaussian functions. Each Gaussian function $(i)$ is described by its width $(\sigma_i)$, its centroid position $(C_i)$, and its area $(A_i)$. The overall centroid position $(C)$ and integrated intensity $(A)$ are then determined by

$$C = \frac{\sum C_i \cdot A_i}{A}, \quad A = \sum A_i \tag{1}$$

**Conventional versus Confocal Micro-XANES.** As mentioned in the introduction section, confocal micro-XANES can be used for surface sensitive analysis, whereas conventional micro-XANES includes also information from the depth of the sample. All confocal micro-XANES spectra are compared to the conventional spectra, qualitatively. For all measurements conventional spectra show no influence of the body, as can be seen for the reproduced sample with grain sizes of 5.5 $\mu$m (C) and firing temperature of 870 °C (1) in Figure 4. The results show that for all measured samples centroid position and integrated intensity of this example are similar to the body. Nevertheless its XANES spectrum can clearly be distinguished from the one of only the body without black glaze on top.

To further affirm the agreement of the two modes, centroid positions and integrated areas of the pre-edge for three spatial positions on the same specimen of modern reproductions and one spatial position on attic pottery were compared quantitatively. Within the uncertainty of the method, confocal micro-XANES and conventional micro-XANES measurements reveal the same results for the centroid position, but confocal micro-XANES reveals 10% smaller integrated intensities. This

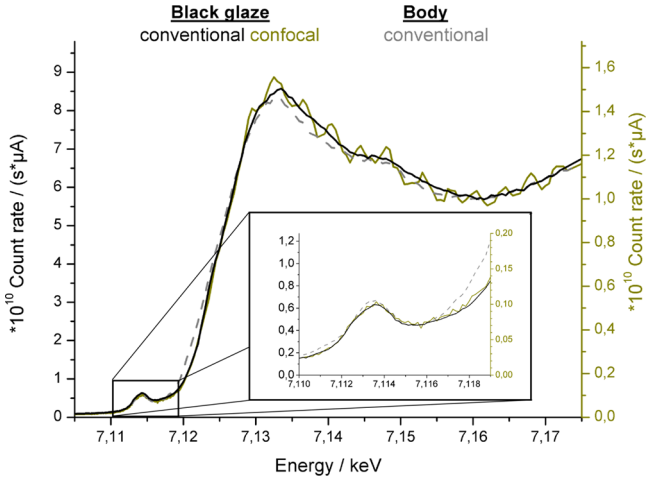


**Figure 4.** Conventional micro-XANES spectrum of black glaze (black) adjusted to the left *y*-axis and a confocal one from the same probing site (ochre) adjusted to the right *y*-axis. The conventional micro-XANES spectrum of the body (gray) is divided by 12.5 to fit it to the left scale.

can also be seen in Table 2, where the calculated integrated areas and the centroid positions of the pre-edge and the

**Table 2. Centroid Position and Ratio of $Fe^{3+}$ to the Total Amount of Iron of Measured and Reconstructed Conventional and Confocal Micro-XANES Spectra of Modern Reproduction C1**

| measurement mode | integrated intensity, eV*a.u. | centroid position ±0.05, eV | $Fe^{3+}/\Sigma Fe^*$ 100%, % |
|---|---|---|---|
| conventional | 0.129 | 7113, 37 | 90 |
| conventional reconstructed | 0.090 | 7113, 36 | 90 |
| confocal | 0.113 | 7113, 36 | 90 |
| confocal reconstructed | 0.107 | 7113, 39 | 90 |

deduced amount of $Fe^{3+}$ are shown for measured and reconstructed spectra for the modern reproduction of Figure 4 (C1). The results of the reconstructed spectra and the calculation of the amount of $Fe^{3+}$ are discussed later.

A precise determination of the integrated intensity of the pre-edge is needed for the estimation of iron coordination. For that purpose both confocal and conventional spectra were corrected for absorption effects. For the correction of the conventional micro-XANES spectra, the open source code FLUO for homogeneous thick samples, which is implemented in the Athena program (iffefit), was used.[24,32]

Confocal micro-XANES spectra were corrected by the reconstruction procedure for stratified samples developed by Lühl et al.[22] The elemental composition used for both correction procedures was determined by SEM-EDX. For the confocal reconstruction, the density has to be known as well. According to previous calculations based on the mole % composition for the ceramic body and the BG and the densities for amorphous silica glass, amorphous alumina, potassium, and Fe(II) oxides, the estimated values are 1.8 and 2.3 g/cm$^3$ for the bulk and the black glaze, respectively.[33]

The differences in the determined integrated intensity are exactly what is expected due to the different self-absorption effects in a homogeneous sample. Due to the limited depth,


dx.doi.org/10.1021/ac500990k | Anal. Chem. 2014, 86, 6924−6930

confocal micro-XANES spectra exhibit less self-absorption effects. In the pre-edge region self-absorption effects cause higher detected intensities in edge-jump normalized spectra. In contrast, the energetic positions of structures are expected to be influenced just to a negligible extend. That means higher self-absorption effects in conventional micro-XANES result in higher integrated intensities but in the same centroid positions as calculated for the example given in Table 2. Hence, for measurements for which the shapes of conventional and confocal micro-XANES spectra are identical, the conventional micro-XANES spectra can be used to determine centroid positions, which simplify the measurement owing to better counting statistics.

Nevertheless, a careful comparison has to be done, especially when measurements have been carried out at positions where the thickness of the black glaze is in the range of 10 $\mu$m (lower limit[14]). In such a case differences between conventional and confocal spectra are expected. For confocal spectra more than 67% of the Gaussian distribution is within the black glaze ($\sigma_x$ − 5 $\mu$m = 9.1 $\mu$m). Due to absorption, the contribution of the black glaze to the detected spectrum is even higher. For conventionally detected spectra, calculations based on the Sherman equation reveal a contribution of less than 30% for the first 10 $\mu$m. In that case the ceramic body has a much higher contribution to the spectra in comparison to the ones detected in confocal mode.

In Table 2 the extracted integrated intensity, centroid position, and determined amount of $Fe^{3+}$ are given for both correction procedures. The centroid position does not change and the integrated intensity decreases in comparison to the one of the measured spectra. In comparison to the conventional absorption correction procedure the confocal reconstruction procedure is less sensitive to variations in elemental composition.[34] This results in a higher reliability in the determined integrated intensities for confocal measurements. For all four samples, for which the correction was carried out, the integrated intensity of the reconstructed confocal spectra is about 20% less than for measured conventional spectra.

**Determination of $Fe^{3+}$ Content.** Wilke et al. determined centroid positions and integrated intensities for iron in minerals[2] and in glass[3] for a large number of reference samples and determined equations to calculate the $Fe^{3+}$ content. For the bulk as well as for the raw material, BG clay paint in modern reproductions iron is expected to be in a mineral phase, whereas for the black glaze of fired ceramics Fe is expected to be present in a mixture of glass and mineral due to the fact that the annealing temperature is substantially lower than the liquidus temperature expected for the reported composition. Thus, both methods for calibration of the pre-edge centroid to determine the $Fe^{3+}$ content for the fired black glaze were applied, and the results compared afterward. Both procedures are briefly introduced below.

For iron in minerals several combinations of coordination ($^{IV}$Fe and $^{VI}$Fe) and oxidation of iron ($Fe^{2+}$ and $Fe^{3+}$) were analyzed by Wilke et al. Before describing the calculation of the $Fe^{3+}/\Sigma Fe$ ratio, considerations on the Fe coordination of our samples are discussed. This is mandatory, because the pre-edge and, thus, the way to obtain the Fe oxidation state depend on the coordination of iron. In Figure 5 the results of the integrated intensities of our samples as well as of the reference samples investigated by Wilke et al. are plotted against the determined centroid positions.

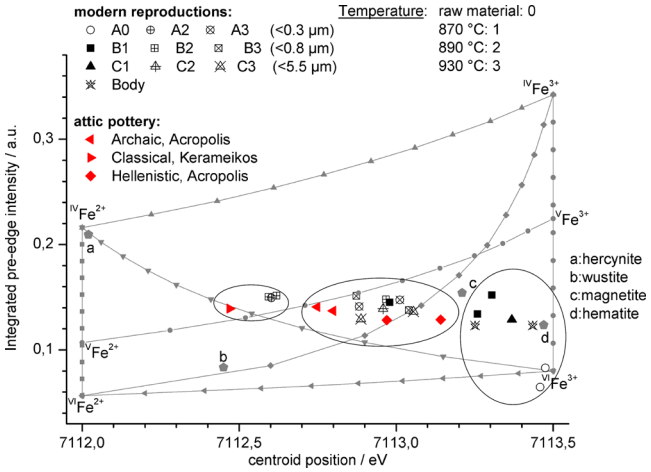


**Figure 5.** Determined integrated intensities and centroid positions of pre-edges of Fe K$\alpha$-XANES spectra for reference material (gray),[2,3] ancient attic BG (red), and modern reproductions (black). For detailed description see also the text.

Gray symbols mark results for reference material. The corners refer to compounds with unique coordination and oxidation state as obtained by Wilke et al. The oxidation state changes from $Fe^{2+}$ (left) to $Fe^{3+}$ (right) and the coordination from $^{IV}$Fe (top) to $^{VI}$Fe (bottom). The gray ticks in between refer to mixtures of the pure end member parameters in 10% steps. For iron in glass the average coordination is always around $^{V}$Fe due to mixtures of IV- and VI-coordinated iron.[3] The gray pentagons (a−d) show Wilke's results for hercynite (a), wustite (b), and magnetite (c), which are formed in the black glaze and hematite (d), which is formed in the bulk during final firing and in the black glaze during the first oxidizing step. Centroid position and integrated intensity of magnetite do not stem from the Wilken et al. publication,[2] where the analyzed natural magnetite was found to be not in the inverse spinel structure due to Ti and Cr contents. This means that part of the $Fe^{2+}$ is found on the tetrahedral lattice site, thus increasing the pre-edge intensity. Results shown here were measured on synthetic magnetite, which shows a fully inverse spinel structure with all $Fe^{2+}$ on the octahedral lattice site, measured at a later beamtime on the HASYLAB beamline A1.

The remaining symbols are our current results calculated from conventional XANES measurements for attic BG (red) and modern reproductions (black). The legend on top allocates the symbols to the different maximum temperature and particle size (in ESD) for modern BG specimens and to the different excavation origins and chronological period of the BG attic pottery.

The integrated intensities for the attic BG and modern reproductions vary between coordination of $^{V}$Fe and $^{VI}$Fe. Including the considerations about self-absorption effects of the previous section, determined integrated intensities for conventional XANES have to be reduced by about 20% resulting in a tendency to $^{VI}$Fe. Due to this considerations and due to the fact that iron in minerals is either four- or six-coordinated, we took the value of $^{VI}$Fe to determine the oxidation state.

With C representing the centroid position in electronvolts, the amount of $Fe^{3+}$ in minerals can be derived by the following equation:[1]


dx.doi.org/10.1021/ac500990k | Anal. Chem. 2014, 86, 6924−6930

$$Fe^{3+}/\sum Fe*100\% = 66.7*(C\text{-}7112) \quad (2)$$

Wilke et al. calibrated the characteristics of the pre-edge of Fe K-XANES to $Fe^{3+}$ amounts of synthetic, slightly simplified basaltic glass systems determined by Mössbauer spectroscopy using the centroid position $C$ (in eV) of the pre-edge:

$$Fe^{3+}/\sum Fe*100\% = [-0.0028 + (0.000784 + 0.00052*(7112 - C))^{0.5}] /-0.00026 \quad (3)$$

## FE OXIDATION STATE OF ATTIC BLACK GLAZE POTTERY

The results of the analysis in terms of centroid position and integrated intensity of the pre-edge for most reduced attic BG pottery and modern reproductions (centroid positions from 7112.4 and 7112.6 eV) are allocated within the triangle formed by wustite, magnetite, and hercynite as can be seen by the data points located in left ellipse (Figure 5), whereas results for raw material samples, the ceramic bulk, and most of the modern reproductions fired at the lowest temperature $T_{max}$ (1: 870 °C) arrange near hematite as indicated by the right ellipse (centroid positions from 7113.3 to 7113.5 eV, see Figure 5).

The calculated contents of $Fe^{3+}$ in different modern specimens are shown in Table 3. For each average ESD (A: <0.3 μm, B: <0.8 μm, and C: <5.5 μm) and maximum firing temperature (0: raw material, 1: 870 °C, 2: 890 °C, and 3: 930 °C) the calculated $Fe^{3+}$ content for both iron in minerals and in glasses is given in percentage values. For the raw unfired BG samples and for the ceramic body, the reference values for iron in glass are not applicable and the corresponding values are marked in italic and were not taken into account for the results in the right column. The results are rounded to 10% values, since the accuracy of the method and the inhomogeneity of the glaze layer down to a microscopic level do not allow for more precise results. Moreover, since the $Fe^{3+}$ content of the black glaze can vary considerably from spot to spot it is recommended to analyze each sample on several spots.

To conclude, a dependence of the $Fe^{3+}$ amount on the firing temperature can be reported: By raising the maximum firing temperature up to 890 °C, the amount of $Fe^{3+}$ decreases. At even higher temperatures ($T_{max}$ 930 °C) the $Fe^{3+}$ amount increases again. Smaller grain sizes lead to lower amounts of $Fe^{3+}$ except for the maximum firing temperature of 930 °C where the $Fe^{3+}$ amount is the same for all ESD values due to incomplete reduction and/or reoxidation at slightly higher temperature.

In Table 4 the results of $Fe^{3+}$ contents from the attic BG are summarized. The most reduced black glaze in this study corresponds to the classical BG sherd (Kerameikos, classical period) presenting high-quality BG with a characteristic bluish-black color. This lowest $Fe^{3+}$ value correlates with the modern BG produced from the finest clay paint (ESD < 0, 3 μm) when fired at $T_{max}$ 890 °C ORO conditions. The results support empirical observations on the quality tests of modern BG pottery produced at THETIS' workshop over a period of 10 years (i.e., since 2003).

**Table 3. Amount of $Fe^{3+}$ in Modern BG Specimens[a]**

| BG Sherd | | method: iron in minerals Fe(III)/% | method: iron in glass Fe(III)/% | result Fe(III)/% |
|---|---|---|---|---|
| A (<0.3 μm) | raw material | 96 | *88* | 100 |
| | | 98 | *92* | |
| | 890 °C | 32 | 24 | 20–30 |
| | 930 °C | 50 | 38 | 40–60 |
| | | 60 | 46 | |
| B (<0.8 μm) | 870 °C | 79 | 64 | 40–80 |
| | | 83 | 68 | |
| | | 57 | 44 | |
| | 890 °C | 31 | 24 | 20–60 |
| | | 33 | 25 | |
| | | 56 | 43 | |
| | 930 °C | 62 | 48 | 40–60 |
| | | 50 | 38 | |
| C (<5.5 μm) | 870 °C | 88 | 75 | 80–100 |
| | | 100 | 99 | |
| | 890 °C | 56 | 43 | 40–60 |
| | | 55 | 42 | |
| | 930 °C | 51 | 39 | 40–60 |
| | | 63 | 49 | |
| body | | 94 | *84* | 80–90 |
| | | 78 | *63* | |

[a]Italicized values were not considered in the calculation of the results (see text).

**Table 4. Amount of $Fe^{3+}$ for the Attic Pottery**

| age | origin | method: iron in minerals Fe(III)/% | method: iron in glass Fe(III)/% | result Fe(III)/% |
|---|---|---|---|---|
| Archaic (6th c. BC) | Acropolis | 41 | 31 | 30–50 |
| | | 45 | 34 | |
| Classical (5th c. BC) | Kerameikos | 24 | 18 | 20 |
| Hellenistic (4th c. BC) | Acropolis | 57 | 43 | 40–70 |
| | | 70 | 55 | |

## CONCLUSION

In the present study we showed and discussed the correlation of the manufacturing technique and the appearance of the black glaze with the amount of $Fe^{3+}$. We compared the surface sensitivity of confocal XANES with higher count rates of conventional XANES. A comparison of spectra of both setups for each measurement position assured that the layer thickness of the black glaze is appropriate for the analysis. This had to be done due to the inhomogeneous nature of the investigated samples. A calculation of the $Fe^{3+}$ amount was done through the analysis of extracted centroid positions of the Fe pre-edge according to methods previously presented for iron in glass and mineral phases. For the calculation of the $Fe^{3+}$ amount for iron in glass, an estimation of the iron coordination was done by means of four reconstructed confocal XANES spectra.

It was verified that the best quality Attic black glaze with the lowest amount of $Fe^{3+}$ results from colloidal clay suspension in water using specific ferruginous illitic clays with grain sizes <0.8 μm and annealing at $T_{max}$ 890–910 °C under ORO conditions. These very narrow criteria for the optimal maximum firing temperature may explain the observed inhomogeneous vitrification of the BG layer since it requires very accurate control of the kiln conditions. The combination of conventional


dx.doi.org/10.1021/ac500990k | Anal. Chem. 2014, 86, 6924–6930

and confocal micro-XANES enabled the semiquantification of the oxidation state of the iron in the black glaze layer only, avoiding any contribution from the bulk substrate, i.e., the ceramic body. This new approach provides the basis for a large-scale analysis involving a wide range of ancient decorated specimens in order to study the development of the ancient manufacturing process in Attica and in other production centers over time.

## ■ ASSOCIATED CONTENT

### Supporting Information

Detailed description of the normalization and background correction of the XANES spectra and additional information about the setup. This material is available free of charge via the Internet at http://pubs.acs.org/

## ■ AUTHOR INFORMATION


### Corresponding Author

*E-mail: Lars.Luehl@physik.tu-berlin.de.

### Present Addresses

[¶]Elettra—Sincrotrone Trieste, Italy.

[‖]ESRF, Grenoble, France.

### Author Contributions

[⊥]These authors contributed equally.


### Notes

The authors declare no competing financial interest.

## ■ ACKNOWLEDGMENTS

The research work presented in this paper was initiated during a first experiment that took place at BESSY II in Nov 2008, in the frame of a collaborative work on "Elemental and structural characterization of ancient Greek glassy nano-materials", between NCSR Demokritos and TU Berlin. The authors acknowledge the support by a number of people in their home institutions; Dr. Ivo Zizak from the $\mu$Spot beamline of BESSY II offered valuable technical support during all experiments; Iphigenia Ed. Nalbani from THETIS authentics LTD was responsible for the manufacturing of laboratory specimens. Dr. A.G. Karydas, Dr. D. Sokaras, and Mrs. V. Kantarellou from NCSR Demokritos contributed during the first experimental run.

## ■ REFERENCES


(1) Waychunas, G. A.; Apted, M. J.; Brown, G. E., Jr. *Phys. Chem. Miner.* **1983**, *10*, 1−9.

(2) Wilke, M.; Farges, F.; Petit, P. E.; Brown, G. E., Jr.; Martin, F. *Am. Mineral.* **2001**, *86*, 714−730.

(3) Wilke, M.; Partzsch, G. M.; Bernhardt, R.; Lattard, D. *Chem. Geol.* **2005**, *220*, 143−161.

(4) Berry, A. J.; O'Neill, H. St. C.; Jayasuriya, K. D.; Campbell, S. J.; Foran, G. J. *Am. Mineral.* **2003**, *88*, 967−977.

(5) Gliozzo, E.; Kirkman, I. W.; Pantos, E.; Turbanti, I. M. *Archaeometry* **2004**, *46* (2), 227−246.

(6) Bardelli, F.; Barone, G.; Crupi, V.; Longo, F.; Maisano, G.; Majolino, D.; Mazzoleni, P.; Venuti, V. *J. Synchrotron Rad.* **2012**, *19*, 661−674.

(7) Oberlies, F. *Naturwissenschaften* **1968**, *55* (6), 277−281.

(8) Longworth, G.; Warren, S. E. *Nature* **1975**, *255*, 625−7.

(9) Schumann, T. *Ber. Dtsch. Keram. Ges.* **1942**, *23*, 408−27.

(10) Hofmann, U.; Theisen, R. *Z. Anorg. Allg. Chem.* **1965**, *341* (3−4), 207−216.

(11) Winter, A. *Technische Beiträge zur Archäologie 1*; Römisches-Germanisches Zentralmuseum Mainz: Mainz, Germany , 1959.

(12) Noble, J. V. *Am. J. Archaeol.* **1960**, *64*, 307−318.

(13) Noll, W.; Holm, R.; Born, L. *Angew. Chem., Int. Ed.* **1975**, *4* (9), 602−613.

(14) Winter, A. *Die Antike Glanztonkeramik: Praktische versuche*; Philip von Zabern: Mainz, Germany, 1978.

(15) Tite, M. S.; Bimson, M.; Freestone, I. C. *Archaeometry* **1982**, *24* (2), 117−26.

(16) Maniatis, Y.; Aloupi, E.; Stalios, A. *Archaeometry* **1993**, *35* (1), 23−34.

(17) Aloupi, E. Nature and Micromorphology of Paint Layers in Ancient Ceramics. Ph.D. Thesis; Ph.D publication Ioannina, 1994; ISBN 960-90007-0-3, pp S 63−111 (available online at http://thesis.ekt.gr/thesisBookReader/id/3643).

(18) Aloupi-Siotis, E. In *Papers on Special Techniques in Athenian Vases*; Lapatin, K., Ed.; The J. P. Getty Publications: Los Angeles, CA, 2008; ppS113−128.

(19) Koningsberger, D. C.; Prins, R. *X-ray absorption: Principles, applications, techniques of EXAFS, SEXAFS, and XANES*; John Wiley and Sons Inc.: New York, 1987.

(20) Malzer, W.; Kanngiesser, B. *Spectrochim. Acta, Part B* **2005**, *60*, 1334−1341.

(21) Mantouvalou, I.; Malzer, W.; Schaumann, I.; Lühl, L.; Dargel, R.; Vogt, C.; Kanngiesser, B. *Anal. Chem.* **2008**, *80*, 819−826.

(22) Lühl, L.; Mantouvalou, I.; Malzer, W.; Schaumann, I.; Vogt, C.; Hahn, O.; Kanngiesser, B. *Anal. Chem.* **2012**, *84*, 1907−1914.

(23) Eisebitt, S.; Böske, T.; Rubensson, J.; Eberhardt, W. *Phys. Rev. B* **1993**, *47*, 14103−14109.

(24) Haskel, D. FLUO: Correcting XANES for self-absorption in fluorescence measurements. In *Computer program and documentation* (online). Available from http://www.aps.anl.gov/xfd/people/haskel/fluo.html 1999, access date: 10/2011.

(25) Pfalzer, P.; Urbach, J.; Klemm, M.; Horn, S.; Denboer, M.; Frenkel, A.; Kirkland, J. *Phys. Rev. B* **1999**, *60*, 9335−93.

(26) Iida, A.; Noma, T. *Jpn. J. Appl. Phys.* **1993**, *32*, 2899−2902.

(27) Erko, A.; Schafers, F.; Firsov, A.; Peatman, W. B.; Eberhardt, W.; Signorato, R. *Spectrochim. Acta, Part B* **2004**, *59* (10−11), 1543−1548.

(28) Erko, A.; Zizak, I. *Spectrochim. Acta, Part B* **2009**, *64* (9), 833−848.

(29) Tang, C. C.; MacLean, E. J.; Roberts, M. A.; Clarke, D. T.; Pantos, E. *J. Archaeol. Sci.* **2001**, *28*, 1015−1024.

(30) Schmitz, S.; Möller, A.; Wilke, M.; Malzer, W.; Kanngiesser, B.; Bousquet, R.; Berger, A.; Schefer, S. *Eur. J. Mineral.* **2009**, *21*, 927−945.

(31) Wolff, T.; Mantouvalou, I.; Malzer, W.; Nissen, J.; Berger, D.; Zizak, I.; Sokaras, D.; Karydas, A.; Grlj, N.; Pelicon, P.; Schütz, R.; Žitnik, M.; Kanngiesser, B. *J. Anal. At. Spectrom.* **2009**, *24*, 669−675.

(32) Ravel, B. ATHENA User's Guide [online], Available from http://cars9.uchicago.edu/ifeffit/BruceRavel/Horae, 2009, access date: 10/2011, version 1.5.

(33) Sokaras, D.; Bistekos, E.; Georgiou, L.; Salomon, J.; Bogovacd, M.; Aloupi-Siotis, E.; Paschalis, V.; Aslani, I.; Karabagia, S.; Anastasios Lagoyannis, A.; Harissopulos, S.; Kantarelou, V.; Karydas, A.-G. *Nucl. Instrum. Methods Phys. Res., Sect. B* **2011**, *269* (5), 519−527.

(34) Lühl, L. *Tiefenaufgelöste Röntgenabsorptionsspektroskopie*. Ph.D. Dissertation [Online], Technische Universität Berlin, April 2012. http://opus4.kobv.de/opus4-tuberlin/frontdoor/index/index/docId/3402 (acccessed Jan 12, 2013).